Analysis of geomembrane whale due to liquid flow through composite liner

Guo, Wei; Chu, Jian; Zhou, Bo; Sun, Liqiang

2015

Guo, W., Chu, J., Zhou, B., & Sun, L. (2016). Analysis of geomembrane whale due to liquid flow through composite liner. Geotextiles and Geomembranes, 44(3), 247-253.

https://hdl.handle.net/10356/82798

https://doi.org/10.1016/j.geotexmem.2015.11.003

Analysis of geomembrane whale due to liquid flow through composite liner

GUO Wei[1], CHU Jian[1], ZHOU Bo[1] and SUN Liqiang[2*]

[1]School of Civil & Environmental Engineering, Nanyang Technological University, 50 Nanyang Ave, Singapore;

[2]State Key Laboratory of Hydraulic Engineering Simulation and Safety, Tianjin University, 92 Weijin Road, Nankai District, Tianjin, China.

[*]Corresponding Author, email: slq0532@126.com.

ABSTRACT

Due to the defects of geomembrane liner (GL), leaking water could infiltrate dry soil below, replace the pore air and thus generate geomembrane whale (GW). An analytical solution is proposed in this paper to analyze the geometry and tensile force of axisymmetric GW. Parametric studies are also conducted to identify the influences from key factors and provide predicting charts for practical usage. It is concluded from the parametric studies that the maximum height and tensile force of GW can be achieved when the GW is just about to be submerged by external water. For a given level of external water, the height, width and tensile force of GW versus volume of leaking water curves are bilinear in a log-log graph, with a higher slope before a turning point but a smaller slope after that, whereas gas pressure in GW has reverse trends. It is also observed in this paper that GL with higher $E\delta$ has a strong capacity to confine the gas pressure and thus generate lower and wider GW with higher tensile force and gas pressure.

KEYWORDS: geosynthetic, geomembrane liner, geomembrane whale

1 INTRODUCTION

The composite liner provides an ideal impermeable layer for the construction of water reservoirs, city wetlands, wastewater lagoons, solid waste disposals and some other projects that need a waterproof liner. The composite liner is usually constructed using a layer of geomembrane liner (GL) over a compacted clay liner (CCL) or a geosynthetic clay liner (GCL). However, water will leak through GL into the bottom dry soil due to the defect of GL. The defect of GL may arise from manufacturing defects, handling of the geomembrane rolls, on-site placement and seaming, placement of drainage gravel over the liner system, traffic on the liner or the overlying protection layer, placement of the waste in a landfill or cleaning of residue from a leachate lagoon and stress cracking as the geomembrane ages (Row, 2012). The water leaking into the dry soil liner will infiltrate the soil and thus replace the pore gas or generate gas due to a microbiological reaction. The gas will then migrate and aggregate underneath the wrinkle or at a high spot below the GL; see step (1) in Figure 1. When sufficient gas aggregates under the GL, gas pressure larger than the hydraulic pressure acts on its top and the GL is lifted from the ground, thus generating a geomembrane whale (GW), as in step (2) in Figure 1. Although generation of GW will release the gas pressure under GL, it will elongate the GL, making it thinner, increasing the risk of failure and reducing the storage ability of the reservoir. Some in-situ test results have been reported by Cao et al. (2015).

Theoretical calculation methods for the leakage rate, Q (m^3/yr), due to the defect of GL have been proposed by many researchers, e.g., Giroud et al. (1989), Giroud et al. (1992), Giroud and Bonaparte (1989a, b), Giroud (1997), Rowe and Booker (1998), Touze-Foltz et al. (1999), Foose et al. (2001), Cartaud et al. (2005), Rowe and Abdelatty (2012), Rowe (2012) and El-Zein et al. (2012). Generally, the leakage rate of water through the GL is a function of the number and size of holes, permeability of the clay liner, water head difference, interface between the geomembrane liner and clay liner beneath, wrinkles of the constructed geomembrane and properties of the reserved wastewater (Rowe 2012). As the topic is relatively large and complex, it will not be covered in this paper. The following discussion assumes that the leakage rate of GL, Q (m^3/yr), is known or has been calculated based on the mentioned theoretical calculation methods. Then, the total volume of leaking water, V_1 (m^3), could be calculated as

$$V_1 = Qt \tag{1}$$

where t is the time of leakage (yr).

The volume of replaced gas in the GW will be the same as the total volume of leaking water, V_1, if the pore gas in the dry soil is assumed to be fully infiltrated by the leaking water (very low ground water level) and neither the gas generated by the microbiological reaction between leaking water and soil nor the water absorbed by the thin clay liner in GCL is ignored. After the replaced gas migrates and aggregates underneath the wrinkle or at a high spot, the volume of the replaced gas will change from V_1 to V_2 because the gas pressure changes from gas pressure P_1 in the ground to gas pressure P_2 underneath the GL. The gas removed from the ground to the bottom of the GL will also have temperature changes that will also influence the volume of gas in the two statuses. The aggregated gas follows the ideal gas law, i.e., $PV = nRT$, where the letters denote pressure (Pa), volume (m^3), amount (in moles), ideal gas constant and temperature of the gas in kelvin (K and 0 ℃ = 273 K), respectively; thus, we have

$$\frac{P_1V_1}{P_2V_2} = \frac{T_1}{T_2} \tag{2}$$

where T_1 and T_2 (units in K) are the temperature of gas before and after replacement, respectively.

In this paper, an analytical solution is proposed to analyze the geometry and tensile force along the GW. Parametric studies are also conducted in this paper to identify the influences from the key factors and provide predicting charts for practical usage. The proposed solution is capable of calculating the axisymmetric GW generated in construction projects on dry soil related to landfills, water reservoirs and lagoons for wastewater treatment.

2 PROPOSED ANALYTICAL METHOD

2.1 Basic Assumptions

In deriving the solutions, the following assumptions need to be made: (1) the GW is an axisymmetric problem; (2) the geomembrane shell is thin, elastic and weightless; (3) the frictions between the geomembrane and soil liner or water are not considered; (4) the soil surface is horizontal and its deformation due to infiltration is not considered; (5) ground water level is very low and thus the same volume of gas is replaced by the same volume of leaking water.

2.2 Theoretical Derivations

A 2D analytical model of an axisymmetric GW could be simplified from a 3D model, as shown in Figure 2(a). The coordinates of the system are set-up with x in the horizontal direction and y in the vertical direction. The origin of this coordinate is taken as the center of the contact edge with the ground surface. The unit weight of the external water and height are written as γ_w and H_w, respectively. The tensile force along the GW is written as T. The height and width of the cross-section of the GW are denoted as H and B, respectively. An infinitesimal small curve with a length of ds at an arbitrary point S (x, y) can be treated as an arc with a radius of r, as shown in Figure 2(b). The angle between the tangential direction at point S (x, y) and the x-axis is denoted as θ. Then, two geometrical differential equations relating θ and the x and y coordinates can be written as shown in Eqs. (3) and (4). The minus sign in Eq. (4) identifies that the integral direction on $S(x, y)$ is along the direction from $y = H$ to $y = 0$. Because the frictions between water/gas and GW or those between GW and the ground surface are neglected, the tension force along the cross-section is constant and thus we have the expression shown in Eq. (5). The hydraulic pressure from stored water acting externally on the GW at a given depth, y, is written as $\beta\gamma_w (H_w - y)$, where $\beta = 1$ when $H_w > y$ and $\beta = 0$ when $H_w < y$. The force equilibrium equations in the normal and tangential directions along the infinitesimal element yield the expression shown in Eq. (6).

$$\frac{dx}{ds} = \cos\theta \tag{3}$$

$$\frac{dy}{ds} = -\sin\theta \tag{4}$$

$$\frac{dT}{ds} = 0 \tag{5}$$

$$\frac{d\theta}{ds} = \frac{1}{T}\left[P_2 - \beta\gamma_w\left(H_w - y\right)\right] \tag{6}$$

2.3 Boundary Conditions

To solve Eqs. (3) to (6), some more boundary conditions related to the tensile forces and geometries have to be established. It should be noted that the reason for generating the GW is because of the elongation and wrinkle of the flexible GL. The final perimeter of GW, L, in the 2D axisymmetric model is elongated from the initial length of the GL (or B in Figure

2(a)) and length of the wrinkle. Their relationships in this axisymmetric analytical model could be expressed as

$$L = (1 + \frac{T}{E\delta})(1 + \varepsilon)B \tag{7}$$

where δ and E are the thickness and elastic modulus of GL, respectively; ε is the ratio of the wrinkle, which could be calculated as the ratio of the initial wrinkle length to the total length of GL.

A free body diagram of the 2D axisymmetric cross-section is presented in Figure 3. Because the tensile force is balanced in the axisymmetric cross-section and along its tangential directions, the direction of tensile forces on the top point is horizontal, as shown in Figure 3(a). The ground surface is horizontal, making the direction of T on the bottom edge also horizontal; see Figure 3(a). Then, the forces on the horizontal direction only involve the external hydraulic pressure and internal gas pressure. The force equilibrium in the horizontal direction between the two forces yields

$$P_2 H = \frac{1}{2}\gamma_w H_w^2 - \frac{1}{2}\eta\gamma_w (H_w - H)^2 \tag{8}$$

where η is the calculation constant and $\eta = 0$ when $H_w < H$; $\eta = 1$ when $H_w > H$.

It can be seen from Figure 2(a) that there is an inflection point on the cross-section at which the curve changes from being concave to convex. Mathematically, it is the point defined as $y = h_i$, at which $d\theta/ds = 0$ in Eq. (6); $d\theta/ds > 0$ when $y > h_i$ and $d\theta/ds < 0$ when $y < h_i$. Substituting $y = h_i$ and $d\theta/ds = 0$ into Eq. (6), we can obtain a balance between internal gas pressure and external hydraulic pressure at this inflection point, as shown in Eq. (9). Note that $\beta = 1$ in this derivation because the inflection point will always be lower than the external water level, or $h_i < H_w$, because the gas pressure in Eq. (6) is always greater than zero, or $P_2 > 0$, if GM could be generated. Figure 3(b) shows a selected free body from the cross-section with y-coordinates ranging from $y = H$ to $y = h_i$. It can be seen that the forces acting on this free body along the horizontal direction involve the internal gas pressure, external hydraulic pressure and tensile forces. By denoting the angle between the tangential direction at the inflection point and the x-axis as θ_i, the force equilibrium along the horizontal direction could yield the expression shown in Eq. (10). Because the problem is axisymmetric, the volume of the GW could be integrated by using Eq. (11).

$$P_2 = \gamma_w (H_w - h_i) \tag{9}$$

$$T(1-\cos\theta_i) = P_2(H-h_i) - \frac{1}{2}\gamma_w\left[(H_w-h_i)^2 - \eta(H_w-H)^2\right] \tag{10}$$

$$V_2 = \int_0^H \pi x^2 dy \tag{11}$$

147

148 *2.4 Iteration Method*

149 By combining Equations (1) to (11), the geometry and tensile force of the GW could be
150 solved by using a computer program. The unit weight and height of stored water, γ_w and H_w,
151 respectively; leakage volume, V_1; wrinkle ratio, ε; elastic modulus, E; and thickness of GL, δ,
152 are taken as inputs. The following two boundary conditions are also adopted for the
153 calculation of the curved section: 1) when $y = H$ and $\theta = 0$ and 2) when $y = 0$ and $\theta = 0$.

154

155 To solve the differential equations, a computer program has been developed using the
156 adaptive Runge-Kutta-Merson method (RKM4), which has already been coded by Press et al.
157 (2007), Xu (1995), Christiansen (1970) and Lukehart (1963). A mathematical programming
158 scheme, the Complex Method proposed by Box (1965), was used to search for the unknown
159 parameters in their specific ranges. For more details of the Complex Method, one can refer to
160 Lipson (1977) and Xu (1995).

161

162 3 **PARAMETRIC STUDIES**

163 *3.1 Influence of external water level*

164 The effects of the external water level are studied to investigate the influence from water
165 level changes that may arise from rainfall, drought, water filling or discharge. The parameter
166 studies are conducted by assuming that the gas pressure P_1 in soil is the standard atmospheric
167 pressure and P_1 = 101.235 *kPa*. The influence from the length of the wrinkle is not
168 considered (ε = 0). The unit weight of stored water is γ_w = 10 kN/m^3. The product of elastic
169 modulus, E, and thickness of GL, δ, is taken as one parameter: $E\delta$ = 300 *kN/m*. The solutions
170 are given for different external water heights, H_w, and different volumes of leaking water, V_1.

171

172 For a certain volume of leaking water, V_1 =300 m^3, three cross-sections of GM with respect to
173 different external water levels were plotted, as shown in Figure 4. To have a better angle of
174 view, the 2D axisymmetric cross-sections are reflected along the y-axis. It can be seen that

when the external water level increases from 2 *m* to 4.9 *m*, the cross-section is protruded, with its width decreased from 8.01 m to 7.31 m, whereas its height increased from 4.03 *m* to 4.93 *m*. This is because the external water level is lower than the height of GW and thus the hydraulic pressure only acts around the GW. If water levels continue to increase, the external water submerges the GW and compresses the width and height of the cross-section. For example, when H_w increased from 4.9 *m* to 10 *m* (Figure 4), the width of the cross-section decreased from 7.31 m to 6.72 m and height from 4.93 *m* to 3.71 *m*.

This phenomenon can be further illustrated through the heights of GW versus external water heights curves, as shown in Figure 5. Generally, for each certain volume of leaking water, V_1, the cross-section of the GWs has one maximum height at which the GW is just about to be submerged by external water. Before this maximum height, the external water protrudes the cross-section and thus makes the height of GW increase nonlinearly with increasing external water level. Take V_1 = 200 m^3 for example; the height of GW increased by a factor of 2.8 from 1.44 to 4.02 when the external water level increased from H_w = 0.2 *m* to H_w = 4 *m*. After the peak, the external water submerged and compressed the GW and thus the height of GW decreased with increasing external water level. Take V_1 = 200 m^3 for example; the height of GW decreased by a factor of 0.62 from 4.02 to 2.51 when the external water level increased from H_w = 4 *m* to H_w = 20 *m*. One more very interesting phenomenon that can be found in Figure 4 is a linear relationship between the maximum heights of GW and height of the external water, with a slope of 1.0 and intercept of 0.0. Figure 6 shows the tensile force along the GW versus height of external water curves. The same trends as those for the height of GW versus external water level curves are observed. The peak values of the tensile forces for different volumes of leaking water are also in a linear relationship with respect to the height of the external water, with a slope of 15.3.

The gas pressure in GW increases nonlinearly with increasing external water height before reaching the peak height of GW but linearly after the peak height; see Figure 7. This is because part of the gas pressure was released and thus protruded GM before it was submerged by the external water. However, after GM was submerged by the external water, the gas was compressed and confined in GM such that its pressure depends on the compression from the hydraulic pressure. The higher the hydraulic pressure, the higher the gas pressure generated. One more phenomenon that could be observed in Figure 7 is that the lower the volume of leaking water, the higher the gas pressure in the GW when all other

conditions are constant. This is because GW is a natural phenomenon that occurs to release the gas pressure. A large volume of GW will release the gas pressure but, at the same time, will increase the tensile force along the GW. Figure 8 shows the width of GW versus height of the external water level curves. It can be seen that the width of GW decreases nonlinearly with increasing external water level. The widths of GW decrease quickly with respect to the external water level before the peak height of GW but slowly after that. This is also consistent with the observations of the external water effects of protruding and compressing.

3.2 Influence of leakage volume

The effect of water leakage volume, V_1, is studied to investigate the influence from leaking time, *t*, and leakage rate, *Q*. The parameter study is conducted by using the same parameters as those used in section 3.1, except that the water leakage volumes range from 1 m^3 to 1000 m^3. The heights of GW versus leakage volume curves in the log-log graph are shown in Figure 9. It can be seen that the curves are bilinear, with high slopes before a turning point and small slopes afterwards. The turning points in these curves indicate the volumes of leakage water when GW is just about to emerge from the external water. It is easy to understand that the deeper the external water, the higher the volume of leakage water required for the GW to emerge from the external water. Take the case of H_w = 2 m, $E\,\delta$ = 300 *kN/m* for example; the turning point is at V_1 = 50 m^3. For the case of H_w = 5 m, E δ = 300 kN/m, the turning point increases to V_1 = 300 m^3. Another phenomenon that can be observed from the two lines is that the GWs are higher for the case of H_w = 2 *m* than for the case of H_w = 5 *m* before V_1 = 50 m^3. This agrees with our expectation that lower hydraulic pressure has lower compression effect on the GW. However, this trend reversed after the volume of leaking water became larger than 50 m^3. The tensile forces along GW versus volumes of leakage water curves in the log-log graph are shown in Figure 10. Generally, the same phenomenon has been observed as those from the height of GW versus volumes of leaking water curves. The widths of GW versus volumes of leaking water curves in the log-log graph are shown in Figure 11. It can be seen that the curves are bilinear, with lower slopes before the turning point and larger slopes afterwards. However, the differences between their slopes are not very clear. The lower external water level also induces a lower width of GW, which is consistent with our expectations. Figure 12 shows the gas pressures versus volumes of leaking water curves in the log-log graph. It can be seen that the gas pressures decrease slowly with increasing volume of leaking water before a turning point and increase heavily afterwards. Take the case of H_w = 5 *m*, $E\,\delta$ = 300 *kN/m* for example; the decreasing rate is

0.054 before V_1 = 200 m^3 and changes to 0.4 after V_1 = 200 m^3. For the case of H_w = 10 *m*, $E\delta$ = 300 *kN/m*, the curve nearly reaches the turning point, which is not plotted in the range of the log-log graph.

3.3 Influence of elastic modulus

The effect from the elastic modulus, E, and thickness of GL, δ, are investigated by taking their product, $E\delta$, as one parameter. Cases of $E\delta$ of 300 *kN/m* and 1000 *kN/m* are studied in the parametric studies. The solutions are given for different external water heights, H_w, and different volumes of leaking water, V_1. As shown in Figure 9, the higher the $E\delta$, the lower the GW generated. This is because a higher $E\delta$ has a strong ability to confine the gas pressure and thus generates lower GW. It can also be seen that a higher $E\delta$ could increase the turning point, or a strong GL needs more gas to emerge from the external water. Take the case of H_w = 2 *m* for example; the turning point for $E\delta$ = *300 kN/m* is V_1 = 50 m^3, but for $E\delta$ = *1000 kN/m*, it increases to V_1 = 100 m^3. A higher $E\delta$ will increase the tensile force along GW, as shown in Figure 10. Their differences are almost constant in the log-log graph before and after the turning points. It is easy to understand that a strong GL could hold the GW at a lower volume, making the gas pressure hard to release (Figure 12) and generating a larger tensile force. A strong GL will also induce wider GW, as shown in Figure 11. With respect to different $E\delta$, the differences between the widths of GW versus leaking water volume curves in the log-log graph are almost constant.

4 **CONCLUSIONS**

Leaking water due to the defects of a geomembrane liner (GL) could infiltrate the dry soil below, replace the pore air and thus generate a geomembrane whale (GW). A new analytical solution was proposed in this paper to analyze the geometry of GW and the tensile force along it. Parametric studies were also conducted in this paper to identify the influences from the key factors and provide designing charts for practical usage

When the water level changes due to rain, drought, water filling or discharge, the maximum height and tensile force of GW can be achieved, at which the GW is just about to be submerged by external water. There is a linear relationship between the maximum heights and tensile force of GW and height of the external water, with slopes of 1.0 and 15.3, respectively. However, the gas pressure in GW continues to increase, whereas the width of GW decreases, with increasing external water level.

The effect of the leakage volume was studied to investigate the influence from leaking time and rate. For a certain external water, the height of GW and tensile force along the GW versus volume of leaking water curves are bilinear in the log-log graph, with higher slopes before the turning point and smaller slopes afterwards, whereas gas pressure in the GW has different trends.

The product of the elastic modulus and thickness of GL, $E\delta$, also influences the tensile force and geometry of GW. A GL with higher $E\delta$ has a strong ability to confine the gas pressure and thus generate lower GW with higher influence on width. However, strong GL will induce higher tensile force along the GW and gas pressure in the GW under same other conditions.

Acknowledgment: Funding support from the Singapore National Research Foundation, Singapore (No. CRP-5-2009-1) and support from other members of the research teams are gratefully acknowledged.

5 NOTATIONS

B	Influence width of cross-section
E	Elastic modulus of GL
H	Height of cross-section
h_i	Height of inflection point
H_w	Height of external water
L	Perimeter of cross-section
P_1	Gas pressure in ground
P_2	Gas pressure in GW
Q	Rate of water leakage through GL
r	Radius of the infinitesimal element
T	Tensile force along GW
t	Time of leakage
T_1	Temperature of gas in soil
V_1	Volume of leaking water
T_2	Temperature of gas in GW
V_2	Volume of gas in GW
γ_w	Unit weight of water
δ	Thickness of GL

ε	Ratio of wrinkle
θ	Angle between x axis and the tangential direction along the curve
θ_i	Value of θ at inflection point

6 REFERENCES

Box, M.J., 1965. A new method of constrained optimization and comparison with other methods. Computer Journal, 8(1), pp. 42-52.

Cartaud, F., Goblet, P., Touze-Foltz, N., 2005. Numerical simulation of the flow in the interface of a composite bottom liner. Geotextiles and Geomembranes 23 (6), 513-533.

Cao, X., Yuan, J., He, G., Liu, Y., Yin, Z., 2015. In situ test and analysis method of air bulging under geomembranes in a shallow-lined reservoir, Geotextiles and Geomembranes, 43(1), pp. 24-34.

Christiansen, J., 1970. Numerical solution of ordinary simultaneous differential equations of the 1st order using a method for automatic step change. Numer. Math. 14, pp. 317-324.

El-Zein, A., McCarroll, I., Touze-Foltz, N., 2012. Three-dimensional finite-element analyses of seepage and contaminant transport through composite geosynthetics clay liners with multiple defects, Geotextiles and Geomembranes, 33, pp. 34-42.

Foose, G., Benson, C., Edil, T., 2001. Predicting Leakage through Composite Landfill Liners. J. Geotech. Geoenviron. Eng., 127(6), pp. 510–520.

Giroud, J.P., 1997. Equations for calculating the rate of liquid migration through composite liners due to geomembrane defects. Geosynthetics International, 4 (3-4), pp. 335-348.

Giroud, J.P., Badu-Tweneboah K., Bonaparte R., 1992. Rate of leakage through a composite liner due to geomembrane defects. Geotextiles and Geomembranes, 11, pp. 1-28.

Giroud, J.P., Bonaparte R., 1989a. Leakage through liners constructed with geomembranes-Part 1. Geomembrane Liners. Geotextiles and Geomembranes, 8, pp. 27-67.

Giroud, J.P., Bonaparte R., 1989b. Leakage through liners constructed with geomembranes-Part 2. Composite Liners. Geotextiles and Geomembranes, 8, pp. 71-111.

Giroud, J.P., Khatami, A., Badu-Tweneboah K., 1989. Evaluation of the rate of leakage through composite liners, Geotextiles and Geomembranes, 8, pp. 337-340.

Lipson, S.L., Gwin, L.B., 1977. The complex method applied to optimal truss configuration. Computers & Structures, 7(3), pp. 461-468.

Lukehart, P.M., 1963. Algorithm 218. Kutta Merson. Comm. Assoc. Comput. Mach., 6(12), pp. 737-738.

Press, W., Teukolsky, S., Vetterling, W., Flannery, B., 2007. Section 17.1 Runge-Kutta Method. Numerical Recipes: The Art of Scientific Computing, Cambridge University Press, New York.

Rowe, R.K. 2012. Short- and long-term leakage through composite liners. The 7th Arthur Casagrande Lecture. Can. Geotech. J., 49, pp. 141–169.

Rowe, R.K., Abdelatty, K. 2012. Modeling contaminant transport through composite liner with a hole in the geomembrane. Can. Geotech. J., 49, pp. 773-781.

Rowe, R.K., Booker, J.R. 1998. Theoretical solutions for calculating leakage through composite liner systems. Geotechnical research centre report. GEOT-18-98.

Touze-Foltz, N., Rowe, R.K. Duquennoi, C., 1999. Liquid flow through composite liners due to geomembrane defects: analytical solutions for axi-symmetric and two-dimensional problems, Geosynthetics International. 6(6), pp. 455-479.

Xu, S.L., 1995. C algorithms commonly used procedures set (2nd edition), Tsinghua University Press, Beijing, China.

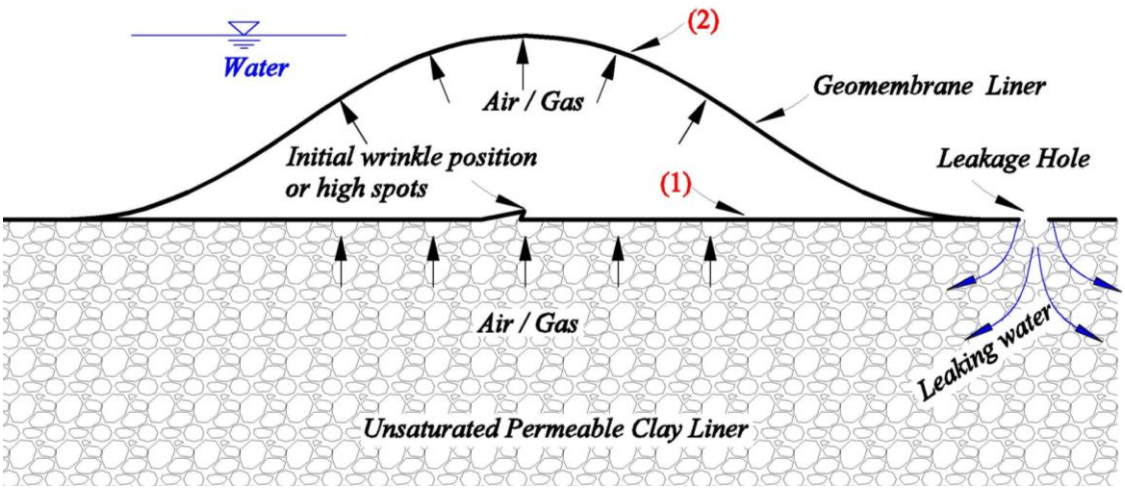

Figure 1 Generation process of GW due to water leakage through GL for (1) Initial position of GL and (2) Final position of GL (GW)

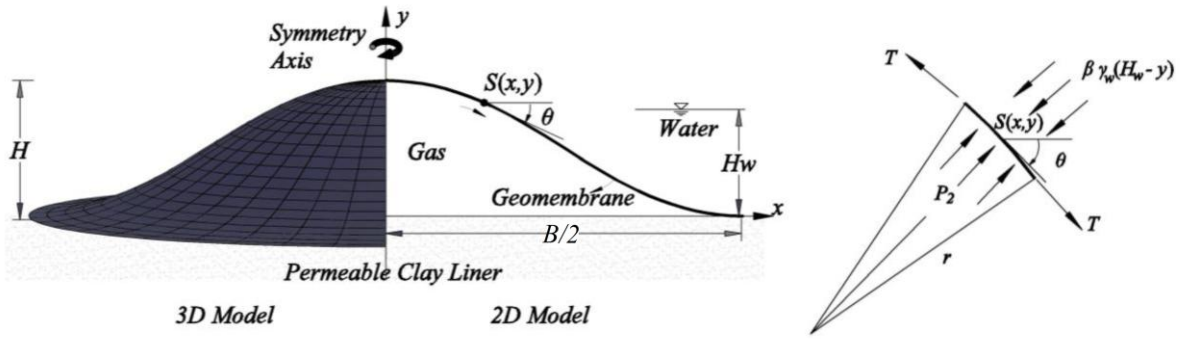

(a) method of simplifying from 3D to 2D model (b) free body diagram of an infinitesimal unit

Figure 2 Simplified analytical model of GW

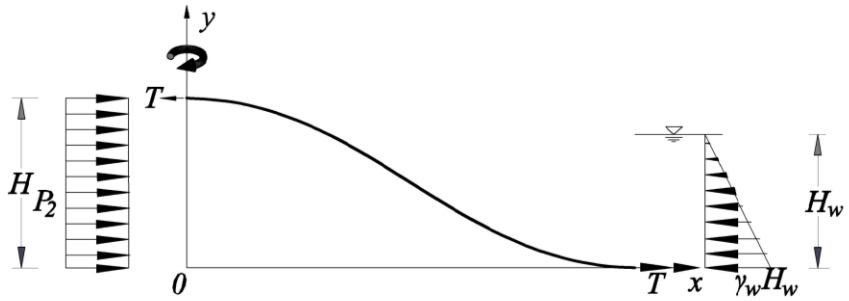

(a) Free body diagram of axisymmetric model

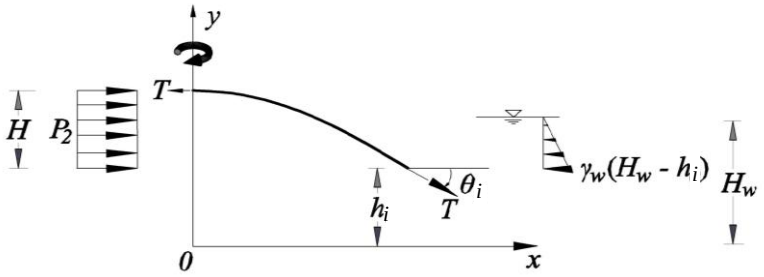

(b) Free body diagram of the selected curve

Figure 3 Free body diagrams for the calculation of boundary conditions

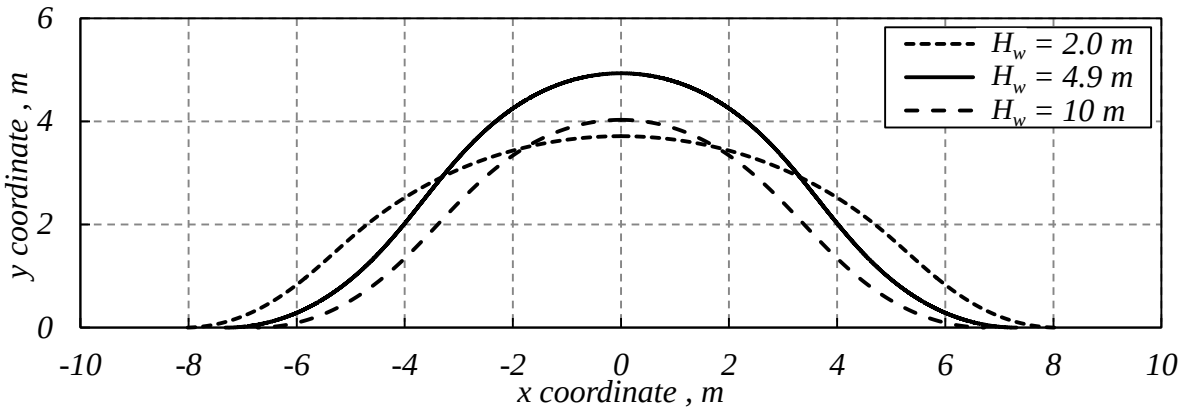

Figure 4 Cross-section of GW with respect to different external water levels

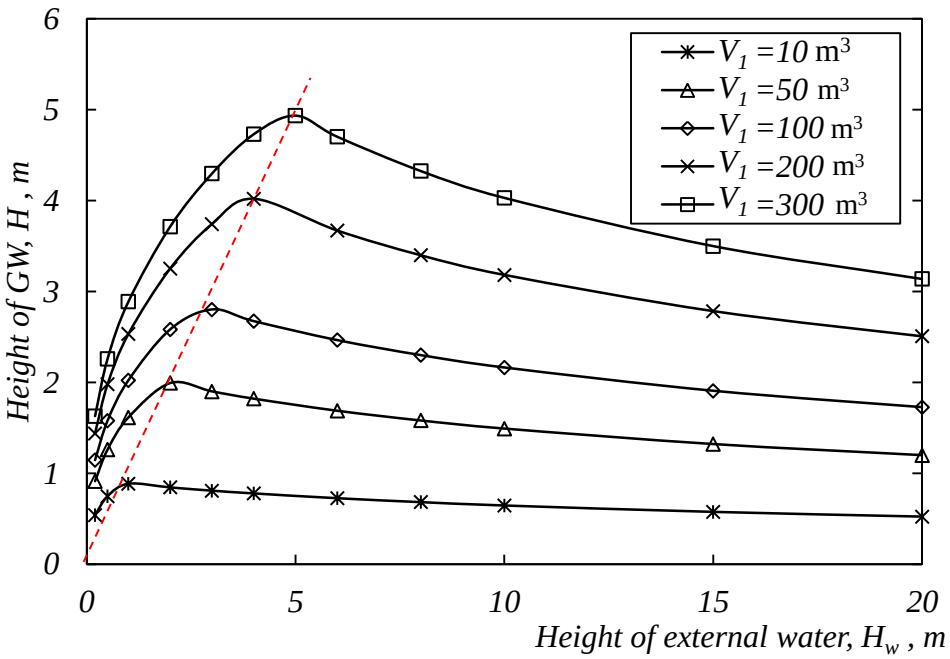

Figure 5 Height of GW vs external water height curves

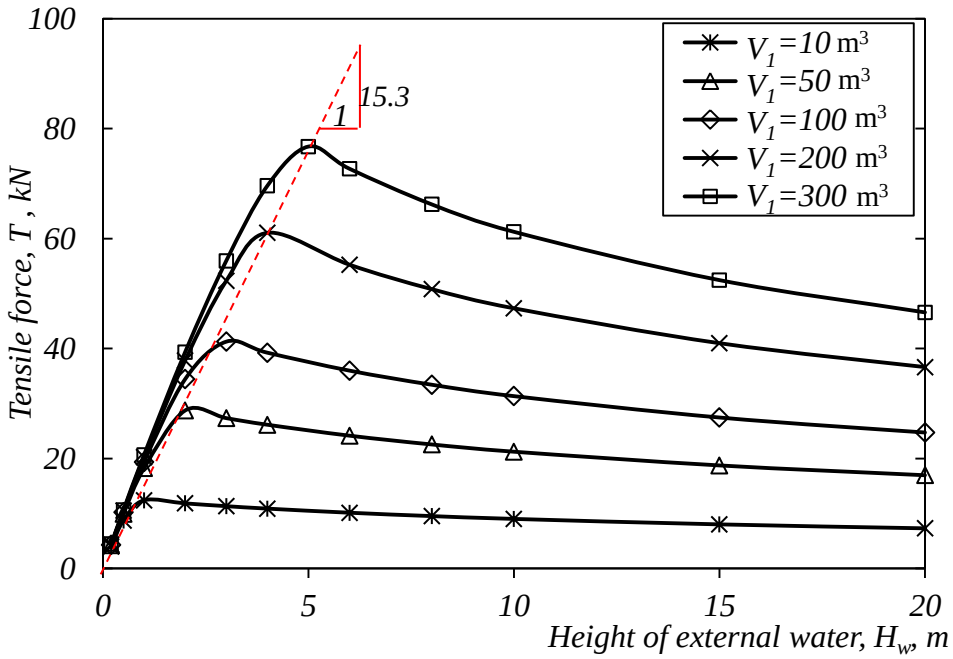

Figure 6 Tensile force along GW versus height of external water curves

401

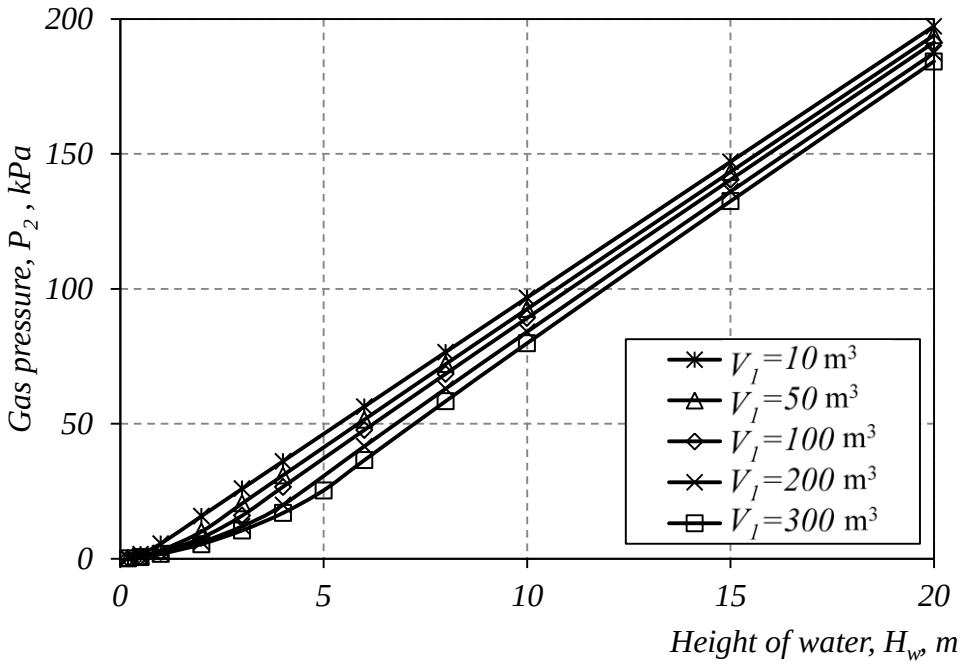

402

403

404 Figure 7 Gas pressure in GW vs height of external water curves

405

406

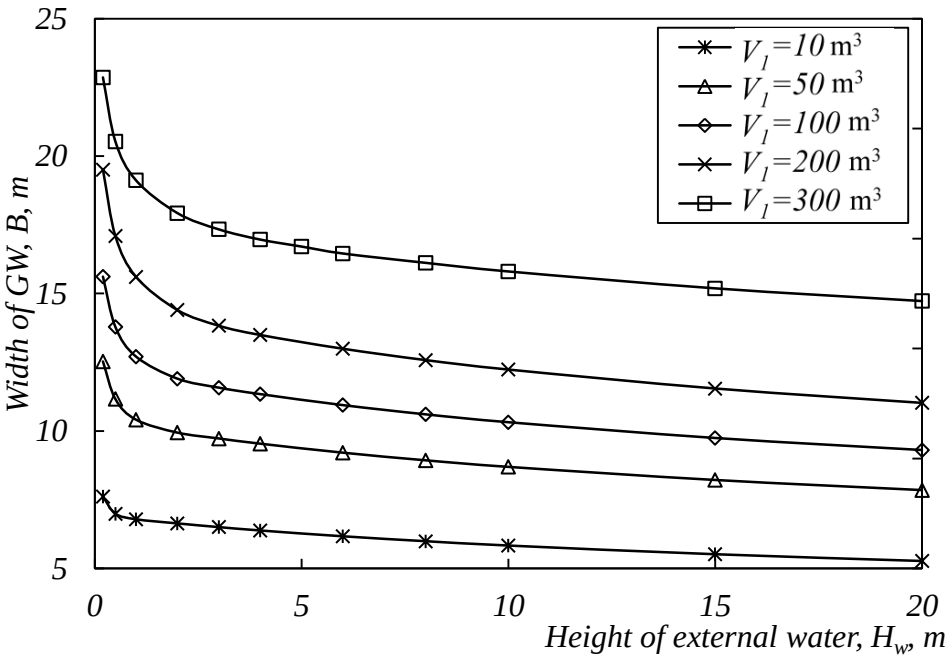

407

408

409 Figure 8 Width of GW vs height of external water curves

410

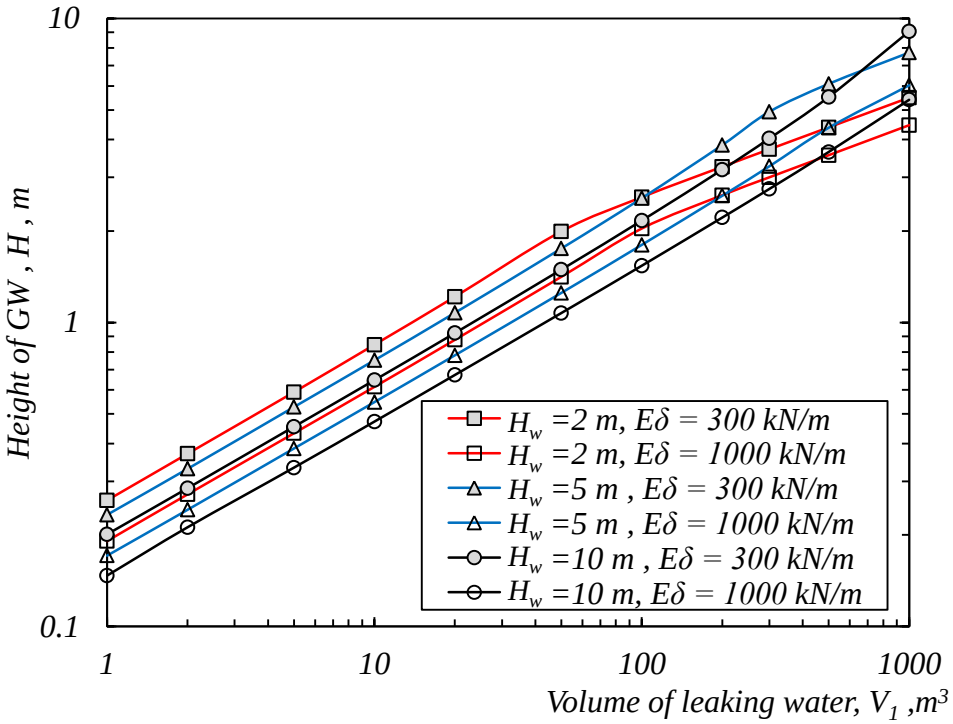

411

412

413 Figure 9 Height of GW vs volume of leaking water curves in log-log graph

414

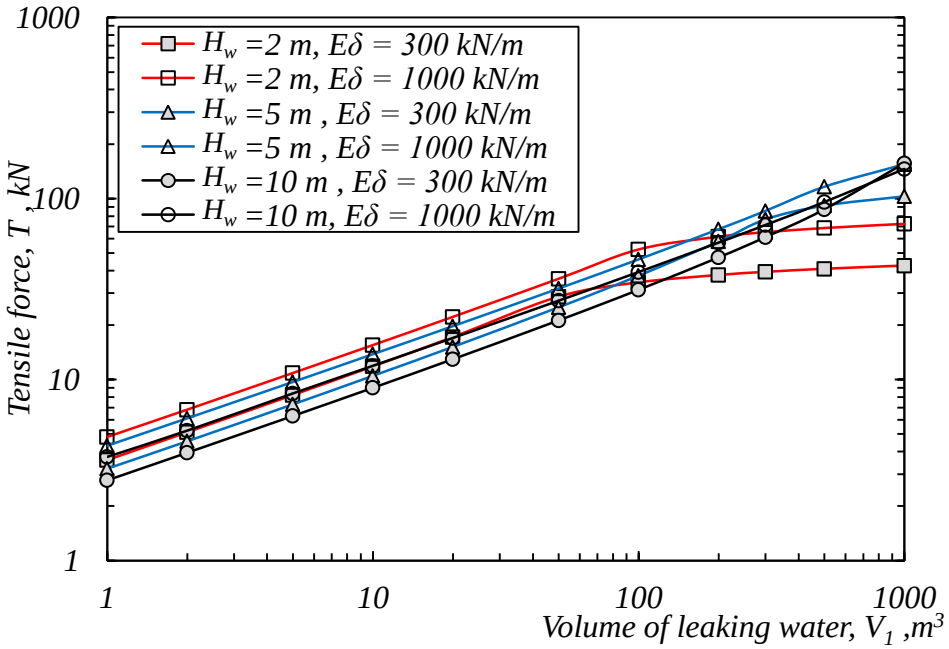

Figure 10 Tensile force of GW vs volume of leaking water curves in log-log graph

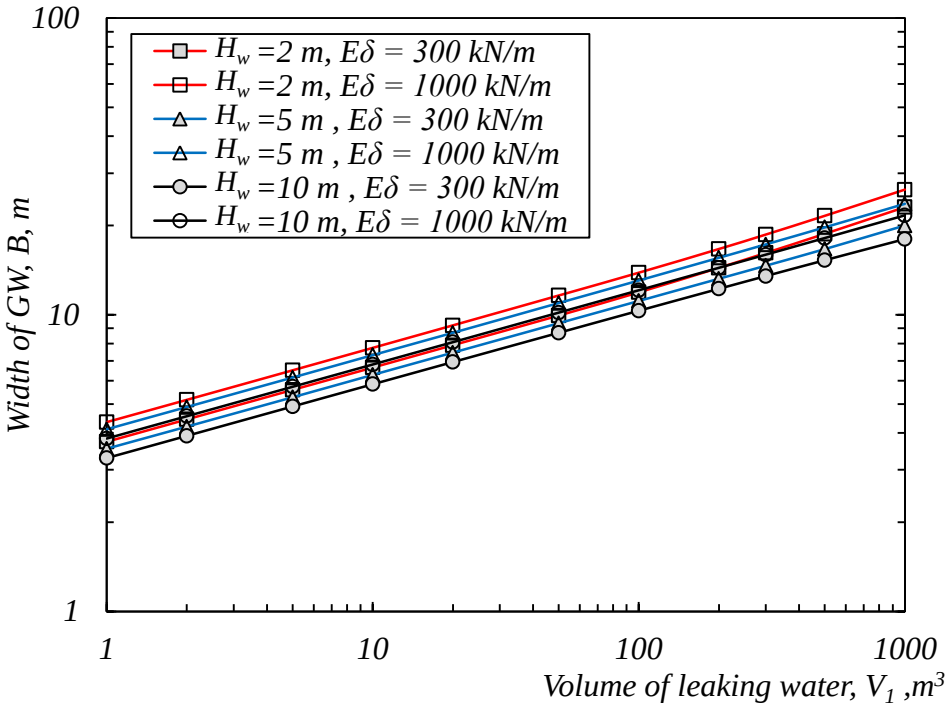

Figure 11 Width of GW vs volume of leaking water curves in log-log graph

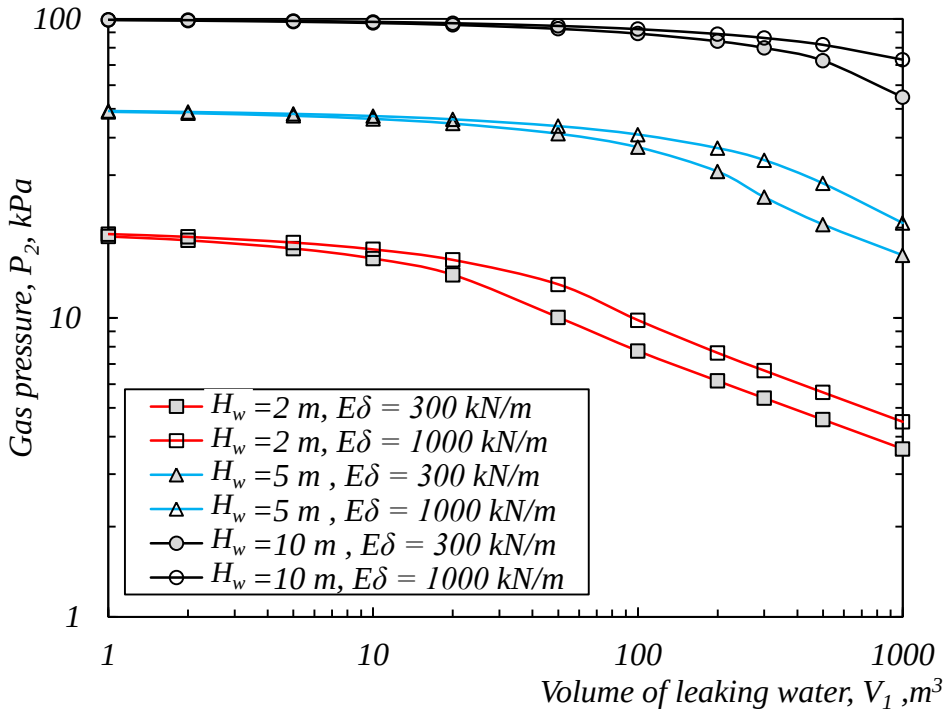

Figure 12 Gas pressure in GW vs volume of leaking water curves in log-log graph